

## HIGH VELOCITY HI IS NOT ASSOCIATED WITH TEV SUPERNOVA REMNANT W51C

W.W. TIAN<sup>1,2</sup>, D.A. LEAHY<sup>2</sup>

*Draft version August 8, 2018*

### ABSTRACT

The recently-detected TeV  $\gamma$ -ray source HESS J1923+141 coincides with Supernova Remnant (SNR) W51C and the star forming region W51B of the W51 complex. We construct HI absorption spectra to SNR W51C, HII regions G49.2-0.35 and G49.1-0.38 in W51B, and a nearby compact extragalactic source. Our study detects high-velocity (HV) HI clouds (above  $83 \text{ km s}^{-1}$ ) which coincide with W51B, but finds that the clouds are behind W51B. Both W51C and G49.2-0.35 have similar highest-velocity absorption features at  $\sim 70 \text{ km s}^{-1}$ . The HII region G49.1-0.38 is behind the SNR because its HI absorption spectrum has a feature at  $83 \text{ km s}^{-1}$ . These new results argue against previous claims that the SNR has shocked the HV HI clouds. Therefore the TeV emission from the complex should not be associated with the HV HI clouds. W51C has a distance of about 4.3 kpc, smaller than the tangent point distance of 5.5 kpc in that direction, but still in the Sagittarius spiral arm.

*Subject headings:* ISM:supernova remnants - ISM:HII regions - ISM:lines and bands - cosmic rays

### 1. INTRODUCTION AND DATA

It is widely known that most Galactic cosmic Rays (CRs) probably originate from supernova remnants (SNRs). Recent studies have supported that young SNRs ( $\sim 1000$  yr old) accelerate charged particles (protons and electrons) in the interstellar medium (ISM) and circumstellar medium (CSM) up to  $10^{15}$  eV (e.g. Bell et al. 2013). However, it is still unclear whether the charged particles emitting the very-high-energy  $\gamma$ -rays are accelerated protons or electrons, i.e. whether the  $\gamma$ -rays are of hadronic origin or of leptonic origin. Recent progress in high energy and Very-High-Energy (VHE)  $\gamma$ -ray observations (Abdo et al. 2010; Helder et al. 2012) and in theoretical investigations (Ohira, Murase and Yamazaki 2011; Li & Chen 2010, Malkov et al. 2011) suggests that the resolution of the hadronic/leptonic ambiguity will soon occur. A key part of this resolution is observation and interpretation of GeV-TeV-bright middle-aged SNRs interacting with molecular clouds.

W51C is one of several such interacting SNRs (W28, W44, W51C and IC443) which have recently been studied in the context of particle acceleration mechanisms (Li & Chen 2012, Aleksic et al. 2012, Fang & Zhang 2010, Abdo et al. 2009). W51C is located in the complex W51, one of the strongest radio sources in the Galaxy. The W51 complex contains components of thermal emission from HII regions (W51A and W51B) and non-thermal emission from SNR W51C (Kassim 1992, Seward 1990). W51C is a strong X-ray emitter (Koo et al. 1995, 2002, 2005; Hanabata et al. 2012). It has been evident that the soft X-rays are thermal and most likely from the SNR interior, and part of the hard X-rays are from a compact object within the SNR, and another part related with stellar winds in the HII regions. Recent  $\gamma$ -ray observations have revealed that the complex is a strong GeV-TeV source (Aleksic et al. 2012), with emission coincident with W51B and W51C but not W51A. It is unknown

whether the VHE emission is associated with the SNR W51C or originates from the star forming region W51B.

In this letter, we use HI absorption lines to study the distances of W51C and the HII regions of W51B and to determine whether high velocity HI is associated with any of these objects. We discuss possible origin of TeV  $\gamma$ -ray emission in the context of the distance results. We utilize the 21 cm continuum and HI line data from the VLA Galactic Plane Survey (VGPS, see details in Stil et al. 2006) in the direction of the W51 complex.

### 2. ANALYSIS AND RESULTS

#### 2.1. Continuum images and Spectra

The methods to extract HI absorption spectrum are detailed in Tian, Leahy & Wang (2007) and Leahy & Tian (2010). In general, the HI absorption spectrum of a radio source can be found by the formula:  $\Delta T = T_{on}^{HI} - T_{off}^{HI} = (T_s^c - T_{bg}^c)(1 - e^{-\tau})$ .  $T_{on}^{HI}$  and  $T_{off}^{HI}$  are the average brightness temperature of many spectra from a selected area on a strong continuum emission region of the target source and an adjacent background region (i.e. excluding the strong continuum emission area).  $T_s^c$  and  $T_{bg}^c$  are the average continuum brightness temperatures for the same regions respectively.  $\tau$  is the optical depth from the continuum source to the observer along the line-of-sight. The main uncertainties in the absorption spectrum are caused by the differences in distribution of small HI clouds along the line-of-sight to source and background regions. Our methods are able to minimize the differences in HI distribution between the source region and the background regions by choosing them to be adjacent.

We show the 1420 MHz continuum image of the W51 complex in Fig. 1. Fig. 1 also shows 3 large ellipses which roughly indicate the areas of W51A W51B and W51C, and 4 small circles where HI-line spectra are extracted. The small circles cover the HII regions G49.2-0.35 and G49.1-0.38 (bright HII regions in W51B), a bright region in W51C, and a nearby compact source (CS) G49.21-0.96.

The HI spectra of the bright HII regions G49.2-0.35 ( $T_B \sim 800$  K) and G49.1-0.38 ( $T_B \sim 255$  K) are shown

<sup>1</sup> National Astronomical Observatories, CAS, Beijing 100012, China. tww@bao.ac.cn

<sup>2</sup> Department of Physics & Astronomy, University of Calgary, Calgary, Alberta T2N 1N4, Canada

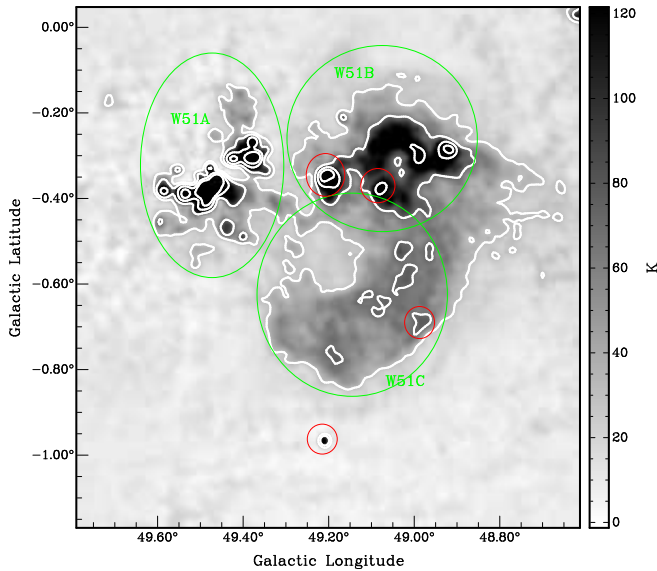


FIG. 1.— The 1420 MHz continuum image of the W51 complex, with contours at 30, 70, 180 and 380 K. W51 A, B and C are indicated by the three large ellipses (green in the online version). The small circles (red in the online version) show the 4 regions from which we extract HI spectra.

in the top panels of Fig. 2. The highest velocity absorption peak is at  $65 \pm 8$  km s<sup>-1</sup> for G49.2-0.35 and at  $75 \pm 8$  km s<sup>-1</sup> for G49.1-0.38. The shapes of the two HI absorption spectra are similar except for the absorption peak at  $75 \pm 8$  km s<sup>-1</sup>, which only appears for G49.1-0.38. Some low  $T_B$  HI clouds ( $\sim 10$  K) with forbidden velocities of 80 – 120 km s<sup>-1</sup> appear in G49.1-0.38’s HI emission spectrum and those at velocity of above 83 km s<sup>-1</sup> have no associated absorption. We calculate absorption column densities from the HI absorption spectra:  $N_{HI} \sim 1.21 \times 10^{22}$  cm<sup>-2</sup> for G49.2-0.35, and  $\sim 1.27 \times 10^{22}$  cm<sup>-2</sup> for G49.1-0.38. We take a typical value of  $T_s = 100$  K,  $N_{HI} = 1.9 \times 10^{18} \tau \Delta v T_s$  cm<sup>-2</sup>, Dickey & Lockman 1990).

The W51C spectrum (3rd panel of Fig.2) is from a faint source so there is much more noise in its absorption spectrum. The main absorption features at 5, 25, 47 and 65 km s<sup>-1</sup> in the HII regions’ absorption spectra are all clearly seen in the W51C spectrum. The highest reliable absorption velocity towards W51C is  $70 \pm 3$  km s<sup>-1</sup>, close to that of G49.2-0.35 and lower than that of G49.1-0.38. The absorption column density of W51C is  $\sim 0.45 \times 10^{22}$  cm<sup>-2</sup>, smaller than that of either G49.2-0.35 and G49.1-0.38. The above two facts show that W51C is likely near to G49.2-0.35 but is in front of G49.1-0.38 (i.e. part of HI clouds in velocity range of 73 - 83 km s<sup>-1</sup> are between W51C and G49.1-0.38).

From the HI spectrum of CS G49.21-0.96 ( $T_B \sim 170$  K, 4th panel of Fig.2), we see two absorption features at velocities of -42 and -53 km s<sup>-1</sup>, which show the source is an extra-galactic source. In addition, the highest velocities of emission ( $T_B \sim 20$  K) and absorption towards the compact source are both at  $79 \pm 4$  km s<sup>-1</sup>. Table 1 summarizes the HI maximum-velocity absorption/emission features of the four sources.

## 2.2. HI Channel maps

The above results are confirmed by the HI emission channel maps. In Fig. 3, we show three selected HI

TABLE 1  
HI ABSORPTION/EMISSION FEATURES OF FOUR SOURCES

Source Name:	G49.2-0.35	G49.1-0.38	W51C	G49.21-0.96
	HII	HII	SNR	nearby CS
$V_{MA}$ (km s <sup>-1</sup> )	$65 \pm 8$	$75 \pm 8$	$70 \pm 3$	$79 \pm 4$
$V_{ME}$ (km s <sup>-1</sup> )	$72 \pm 8$	$\geq 115$	$70 \pm 8$	$79 \pm 4$

$V_{MA}$ : maximum absorption velocity,  $V_{ME}$ : maximum emission velocity.

channel maps towards the W51 complex. HI absorption towards G49.1-0.38 appears (seen as the low  $T_B$  white spot) in the channel maps for velocities 80.98 km s<sup>-1</sup> or less, but not for velocities 85.93 km s<sup>-1</sup> or higher. The HI absorption towards G49.2-0.35 appears in the 73.56 km s<sup>-1</sup> (and lower) channel maps but not in the higher velocity maps. The channel map at 80.98 km s<sup>-1</sup> shows several high- $T_B$  HI clouds extending across W51B, W51C and G49.21-0.96 which show no spatial coincidence with the W51C SNR shell. We conclude this gas is not related with the SNR shock. The channel maps at velocities above 83 km s<sup>-1</sup> (like the map shown for 86 km s<sup>-1</sup>) reveal that the high velocity (HV) HI clouds overlap W51B but do not produce any associated HI absorption towards either G49.1-0.38 or G49.2-0.35. This indicates that the HV HI gas is further than either G49.1-0.38 or G49.2-0.35.

## 3. DISCUSSION AND CONCLUSION

### 3.1. Distances of W51C and HII regions G49.2-0.35 and G49.1-0.38

The most distant reliable absorption features observed against the complex W51B and W51C are at 83 km s<sup>-1</sup> for G49.1-0.38 and 73 km s<sup>-1</sup> for both W51C and G49.2-0.35. They are much greater than the maximum velocity (i.e. tangent point velocity) of  $V_T \sim 62$  km s<sup>-1</sup> permitted by the flat Galactic circular rotation curve model (taking the recently-measured parameters of  $V_0 = 254 \pm 16$  km s<sup>-1</sup>,  $R_0 = 8.4 \pm 0.6$  kpc by VLBI observations, Reid et al. 2009) in the direction of  $l = 49.2^\circ$ . However, the additional velocity of  $\sim 10$  km s<sup>-1</sup> could be due to peculiar motions (e.g. spiral arm velocity perturbations; streaming and random gas motions). In this case, we estimate  $V_T \sim 75$  km s<sup>-1</sup> by comparing with the HI background emission spectrum towards  $l = 49.2^\circ$  (which is also consistent with the high velocity-resolution Galactic Arcicibo L-band Feed Array survey data, GALFA<sup>3</sup>). Then the absorption features in the velocity range of 75 to 83 km s<sup>-1</sup> (see HI absorption spectra of G49.1-0.38 and G49.21-0.96) are likely produced by the HI gas in the Sagittarius spiral arm with additional peculiar motions of 8 km s<sup>-1</sup> (Xu et al. 2009, Shaver et al. 1982).

It is difficult to determine accurate distances to Galactic objects without better knowledge of the rotation curve and non-circular motions. For a simplicity, we estimate the kinematic distances to this complex using a flat rotation curve: i.e 254 km s<sup>-1</sup>,  $R_0 = 8.4$  kpc, also considering  $V_R$  linearly increasing to 267 km s<sup>-1</sup> as  $R$  decreases to its value at the tangent point ( $R_T = 6.4$  kpc). Our results are: G49.1-0.38 is located at the far side of its Radio Recombination Lines (RRL) velocity ( $V_{RRL} = 67.9$

<sup>3</sup> <http://www.naic.edu/~igalfa>

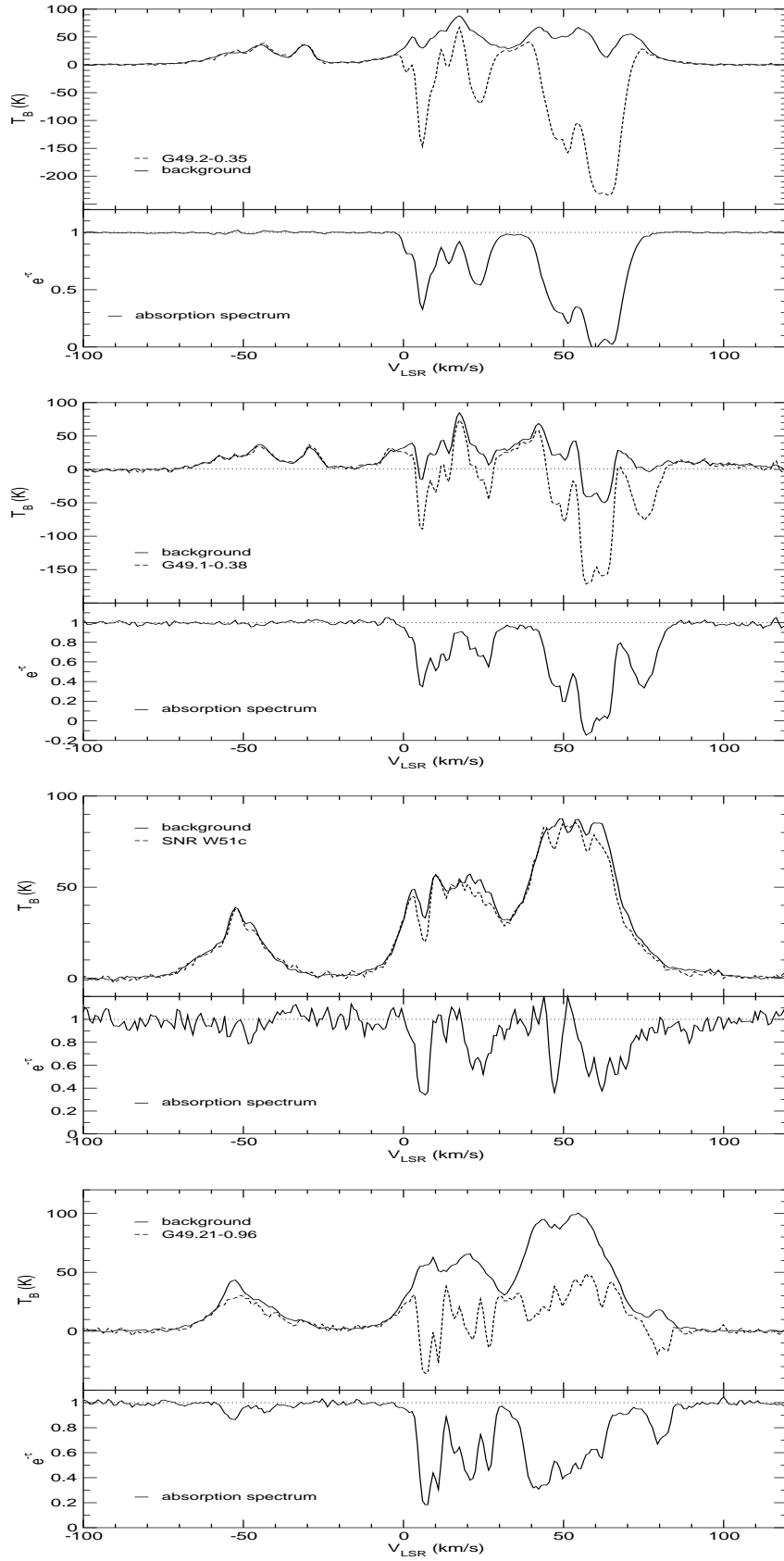


FIG. 2.— HI emission (upper half of each panel) and respective HI absorption (lower half of each panel) of the two HII regions G49.2-0.35 and G49.1-0.38, of SNR W51C and of the extragalactic compact source G49.21-0.96.

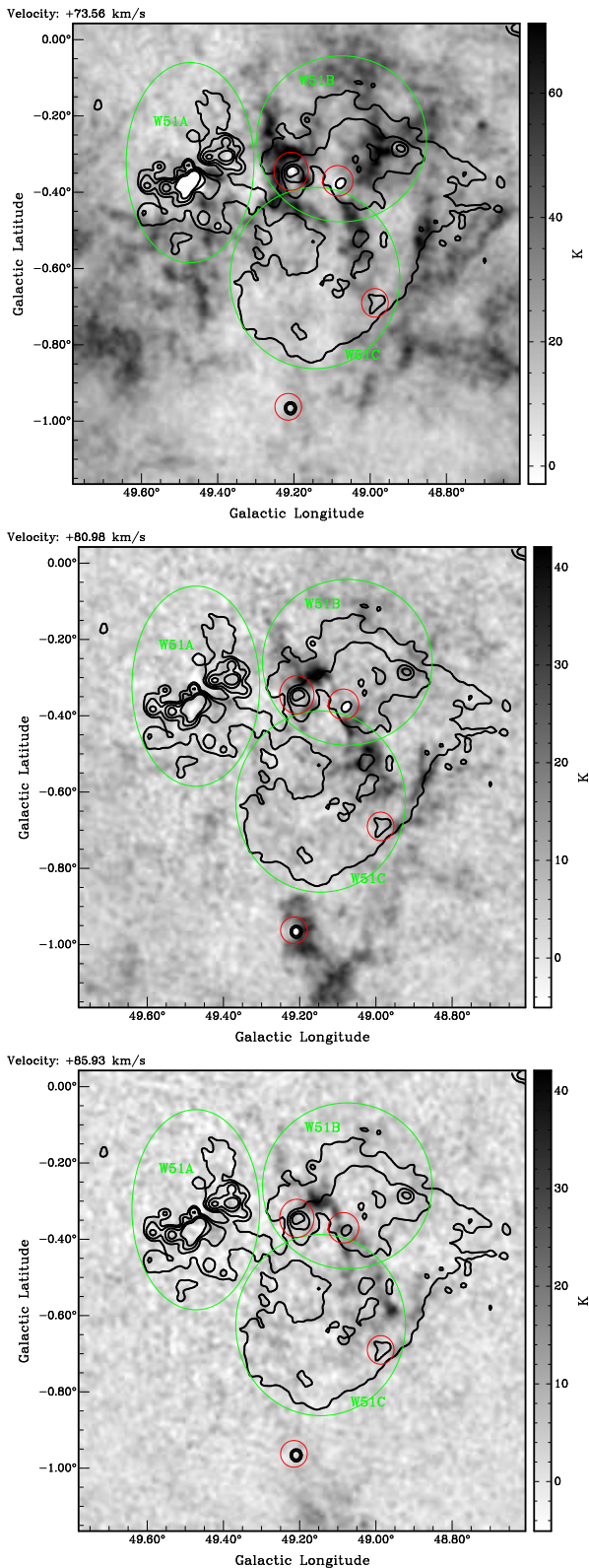


FIG. 3.— The panels show the HI channel maps at velocities of 73, 81 and 86  $\text{km s}^{-1}$  (velocity label at top left of each panel). Overlaid in all panels is the 1420 MHz continuum emission with contours at 30, 70, 180, 380 K. The HI map above 83  $\text{km s}^{-1}$  shows high-velocity extended HI clouds overlapping W51B (see text for detail).

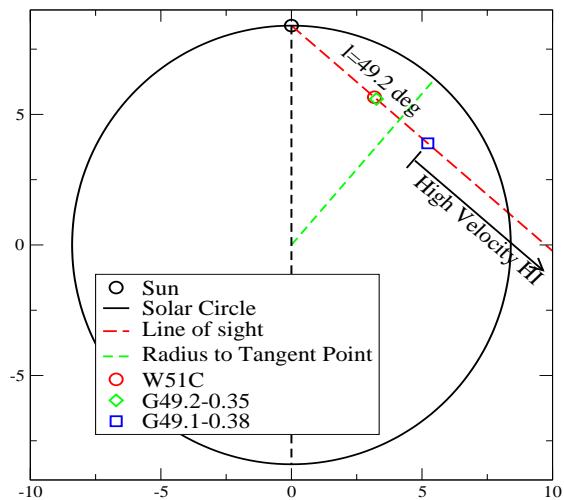


FIG. 4.— Diagram indicating the locations of SNR W51C and HII regions G49.1-0.38 and G49.2-0.35. The possible range of distance for the (unknown) position of the high velocity HI is indicated by the arrow.

$\text{km s}^{-1}$ , Lockman 1989), i.e. at 6.9 kpc, because of the HI absorption feature at the tangent point. G49.2-0.35's highest absorption velocity of  $65 \pm 8 \text{ km s}^{-1}$  is consistent with its  $V_{RRL}$  ( $67.2 \pm 1 \text{ km s}^{-1}$ , Lockman 1989) and is smaller than the tangent point velocity. Also two OH masers associated with G49.2-0.35 have velocities of 69.2 and 72.1  $\text{km s}^{-1}$  (Green et al. 1997, Hewitt et al. 2008). Thus G49.2-0.35 is at the near side distance for the averaged maser velocity of 70.7  $\text{km s}^{-1}$ , i.e., at 4.3 kpc. W51C's highest absorption velocity is  $\approx 70 \text{ km s}^{-1}$  thus it is likely close to G49.2-0.35, so its distance is approximately at 4.3 kpc too. But W51C should be in front of G49.2-0.35 because of its lower column density. The line-of-sight at  $l=49.2^\circ$  goes through the Sagittarius arm and has about 3 kpc length inside the arm (see Figs. 9 and 10 of Hou et al. 2009). The tangent point distance at  $l=49.2^\circ$  is at 5.5 kpc (also see Sato et al. 2010), so both W51C and G49.2-0.35 should be located at near side of the 3 kpc path while G49.1-0.38 is at far side. This is consistent with previous claims that the W51 complex, as an active star forming region, is located in the Sagittarius spiral arm.

The above leads to the following geometrical relation: SNR W51C and the HII region G49.2-0.35 are at 4.3 kpc and the HII region G49.1-0.38 is at 6.9 kpc, well behind them but still within the solar circle. Fig. 4 here illustrates the arrangement of W51C and the HII regions along the line-of-sight at  $l=49.2^\circ$ .

An HI 21-cm absorption line study on the W51 complex has previously been done employing VLA and Arecibo 305m data (Koo 1997, Koo & Moon 1997). Koo (1997) obtained HI absorption spectra of both G49.2-0.35 and G49.1-0.38 (see his Fig. 3 with source names G49.2-0.3 and G49.1-0.4), which are roughly consistent with our spectra (Fig. 2) except the data quality is poorer (lower sensitivity and velocity resolution). We detect both the major HI absorption peak at  $\approx 65 \text{ km s}^{-1}$  for G49.2-0.35, and the highest velocity absorption peak of  $\approx 75 \text{ km s}^{-1}$  for G49.1-0.38. The systemic velocity of HII G49.2-0.35

revealed by the RRL ( $67.2 \text{ km s}^{-1}$ ) and recent CO observations ( $71.2 \text{ km s}^{-1}$ , clump A of Ceccarelli et al. 2011) is associated with the HI absorption feature at  $65 \pm 8 \text{ km s}^{-1}$ . The RRL velocity of  $67.9 \text{ km s}^{-1}$  towards G49.1-0.38 is smaller than its highest HI absorption velocity of  $\simeq 75 \text{ km s}^{-1}$ . This can be simply explained because G49.1-0.38 is at the kinematic far side for its velocity of  $67.9 \text{ km s}^{-1}$ . This is consistent with our above conclusion that G49.1-0.38 is behind of G49.2-0.35, because the HI gas between them produces the HI absorption feature at  $75 \pm 8 \text{ km s}^{-1}$  in the G49.1-0.38 absorption spectrum.

### 3.2. *Is the W51C SN shock interacting with any HI or molecular clouds?*

Previous work has shown HI absorption from HI clouds, with similar  $T_B$  to the HV HI here, is clearly detectable (Fig.2d of Tian & Leahy 2012, Fig. 1d of Tian & Leahy 2008). The HV HI patch is not detected in the absorption spectrum of G49.1-0.38 (Fig. 2, second panel), implying that it is behind G49.1-0.38.

Koo and Moon (1997) claimed detection of high-velocity HI gas with velocities of  $85 \sim 180 \text{ km s}^{-1}$  towards W51B (including G49.2-0.35 and G49.1-0.38, see Fig. 4 of their paper). We confirm detection of emission from the HV (with velocity  $83 \text{ km s}^{-1}$  and higher) HI patch toward G49.1-0.38 (Fig. 2, second panel) but it is not seen toward G49.2-0.35 (Fig. 2, first panel, and Fig. 3, last panel). Our result is consistent with new HI data from the GALFA survey.

Our HI absorption spectra clearly reveal reliable HI absorption features in the velocity range of  $0$  to  $70 \pm 3 \text{ km s}^{-1}$  for W51C and  $0$  to  $65 \pm 8 \text{ km s}^{-1}$  for G49.2-0.35 but not beyond  $73 \text{ km s}^{-1}$  for both sources. This reveals that W51C is at approximately the same distance as G49.2-0.35. The CO clump (A) at the velocity of  $71.2 \text{ km s}^{-1}$  sitting at the core of the HII region G49.2-0.35 (Ceccarelli et al. 2011; also Carpenter & Sanders 1998) is likely associated with the  $65 \pm 8 \text{ km s}^{-1}$  HI absorption feature towards G49.2-0.35. Thus it is possible that there exists an interaction between the W51C shock and the CO clump associated with HII G49.2-0.35. Because the HV HI gas is behind G49.1-0.38, which is far behind G49.2-0.35 and CO clump A, there is no interaction between W51C and the HV HI gas. If we still believe the HV HI gas is caused by shocks, it is more reasonable to believe that the shock is from stellar winds from the star forming region, i.e. HII region G49.1-0.38.

### 3.3. *Are the OH masers from a SN Shock or from a star forming region?*

Two 1720 MHz OH masers are coincident with or adjacent to the HII region G49.2-0.35 within W51B (see Fig. 1 of Brogan et al. 2000). The velocities of the masers ( $69.2$  and  $72.1 \text{ km s}^{-1}$ ) are consistent with the RRL velocity ( $67.2 \pm 1 \text{ km s}^{-1}$ ) and the highest HI absorption velocity ( $65 \pm 8 \text{ km s}^{-1}$ ) of G49.2-0.35. So it is reasonable that the OH masers are associated with G49.2-0.35. The masers are located near the interface between SNR W51C and G49.2-0.35 based on ROSAT X-ray observations of W51B and W51C, although the interface is not obvious (Koo & Kim 1995). 1720 MHz OH masers can be produced either in SNR-shocked clouds or in star forming regions (SFR) under similar conditions (Green et al. 1997, Wardle 1999, Caswell 2004). However, they

have different pumping schemes: the SNR 1720 MHz OH maser seems to be the sole maser transition of OH with corresponding broad OH absorption at 1667, 1665 and 1612 MHz, while the SFR maser most commonly accompanies emission at the 1665 MHz OH transition. Hewitt et al.(2008, 2006) give examples: the 1720 MHz OH masers within the middle-aged /SNRs W28, W44 and IC443 are clearly associated with SNR shocks interacting with adjacent molecular clouds. But for W51C, there is 1665 MHz emission at  $74 \text{ km/s}$ , which indicates that the OH MHz masers likely originate from SFR activity. Many SFR 1720 MHz OH masers are accompanied by the 6035 MHz OH masers (Caswell 2004, Etoka et al. 2012), so additional 6035 MHz maser observations of W51C may help strengthen our conclusion.

Koo et al. (2010) made an HI Zeeman observation of the shocked HV HI gas of W51B and obtained a line-of-sight magnetic field of  $B_{LOS} \leq 0.15 \text{ mG}$  in the HV HI gas (above  $85 \text{ km s}^{-1}$ ). Brogan et al. (2000) measured the  $B_{LOS}$  of  $1.5 \sim 1.9 \text{ mG}$  in the 1720 MHz OH maser gas overlapping W51B. This difference is easily understood if we believe the HI HV gas is not related with the OH maser gas, i.e. they are physically separated. This supports our above conclusion that the HV HI gas is behind the HII region G49.1-0.38.

### 3.4. *Conclusion*

We have used HI absorption spectra to determine the distances to W51C (4.3 kpc) and the HII regions G49.2-0.35 (4.3 kpc) and G49.1-0.38(6.9 kpc). We also consider whether W51C is interacting with atomic gas. This is of interest because GeV and TeV emissions have been detected recently (Abdo et al. 2009) from the area where W51B and W51C overlap. TeV emission from several middle-aged SNRs interacting with adjacent molecular clouds has been considered to originate from hadronic processes (e.g. Ohira et al. 2011). However for W51C, we have found it not interacting with any HV HI. Also we find that the observed nearby OH masers from dense molecular gas are likely associated with the star forming regions in W51B and not W51C. These new results show clear absence of evidence of molecular or atomic gas interacting with W51C, thus casting doubt on a hadronic origin for the GeV/TeV emission from W51C. We think W51C is similar to the case of Tycho SN 1572 (Tian & Leahy 2011), where the SNR was found not to interact with molecular or HI clouds.

WWT thanks the NSFC and China Ministry of Science and Technology under State Key Development Program for Basic Research for support. DAL acknowledge support from the Natural Sciences and Engineering Research Council of Canada. We thank Drs. Gibson and Koo for providing GALFA data. This publication is partly supported by a grant from the John Templeton Foundation and National Astronomical Observatories of the CAS. The opinions expressed in this publication are those of the authors do not necessarily reflect the views of the John Templeton Foundation of NAOCAS. The funds from John Templeton Foundation were awarded in a grant to The University of Chicago which also managed the program in conjunction with NAOCAS. Finally, we thank the referee for suggestions which improved this

paper.

#### REFERENCES

- Abdo, A.A., Ackermann, M., Ajello, M. et al. 2010, *Science*, 327, 1103
- Abdo, A.A., Ackermann, M., Ajello, M. et al. 2009, *ApJ*, 706, 1
- Aleksic, J., Alvarez, E.A., Antonelli, L.A. et al. 2012, *A&A* 541, 13
- Bell, A.R., Schure, K.M., Reville, B., Giacinti, G. 2013, *MNRAS*, accepted. arXiv:1301.7264
- Brogan, C. L., Frail, D.A., Goss, W.M., Troland, T.H. 2000, *ApJ*, 537, 875
- Carpenter, J.M., Sanders, D.B. 1998, *AJ*, 116, 1856
- Caswell, J.L. 2004, *MNRAS*, 349, 99
- Ceccarelli, C., Hily-Blant, P., Montmaerle, T. et al. 2011, *ApJ*, 740, 4
- Dickey, J.M., Lockman, F. J. 1990, *Annu. Rev. A&A*, 28, 215
- Etoka, S., Gray, M.D., Fuller, G.A. 2012, *MNRAS*, 423, 647
- Fang, J., Zhang, L. 2010, *MNRAS*, 405, 462
- Green, A.J., Frail, D. A., Goss, W. M., Otrupcek, R. 1997, *AJ*, 114, 2058
- Hanabata, Y., Sawada, M., Katagiri, H. et al. 2012, *PASJ*, accepted. ArXiv1212.1993
- Helder, E.A., Vink, J., Bykov, A.M. et al. 2012, *Space Science Reviews*, 173, 369
- Hewitt, J.W., Yusef-Zadeh, F., Wardle, M. 2008, *ApJ*, 683, 189
- Hewitt, J.W., Yusef-Zadeh, F., Wardle, M. et al. N.E. 2006, 652, 1288
- Hou, L.G., Han, J.L., Shi, W.B. 2009, *A&A*, 499, 473
- Kassim, N.E., 1992, *AJ*, 103, 943
- Koo, B.C., Kim, K.T., Seward, F.D. 1995, *ApJ*, 447, 211
- Koo, B.C., Moon, D.S. 1997, *ApJ*, 475, 194
- Koo, B.C. 1997, *ApJS*, 108, 489
- Koo, B.C., Heiles, C., Stanimirovi., S., Troland, T. 2010, *AJ*, 140, 262
- Koo, B.C., Lee, J.J. 2002, *AJ*, 123, 1629
- Koo, B.C., Kim, K.T., Seward, F.D., Lee, J.J. 2005, *ApJ*, 633, 946
- Leahy, D.A., Tian, W.W. 2010, *ASPC*, 438, 365
- Li, H., Chen, Y. 2010, *MNRAS*, 409, L35
- Li, H., Chen, Y. 2012, *MNRAS*, 421, 935
- Lockman, F.J. 1989, *ApJS*, 71, 469
- Malkov, M.A., Diamond, P.H., Sagdeev, R.Z. 2011, *Nature Communications*, 2, 194
- Ohira, Y., Murase, K., Yamazaki, R., 2011, *MNRAS*, 410, 1577
- Reid, M.J., Menten, K.M., Zheng, X.W. et al. 2009, *ApJ*, 700, 137
- Sato, M., Reid, M.J., Brunthaler, A., Menten, L.M. 2010, *ApJ*, 720, 1055
- Seward, F.D. 1990, *ApJS*, 73, 781
- Shaver, P.A., Radhakrishnan, V., Anantharamaiah, K.R. et al. 1982, *A&A*, 106, 105
- Stil, J.M., Taylor, A.R., Dickey, J.M. et al. 2006, *AJ*, 132, 1158
- Tian, W.W., Leahy, D.A., Wang, Q.D. 2007, *A&A*, 474, 541
- Tian, W.W., Leahy, D.A. 2008, *ApJ*, 677, 292
- Tian, W.W., Leahy, D.A. 2011, *ApJL*, 729, 215
- Tian, W.W., Leahy, D.A. 2012, *MNRAS*, 421, 2593
- Xu, Y., Reid, M.J., Menten, K.M. et al. 2009, *ApJ*, 693, 413
- Wardle, M. 1999, *ApJ*, 525, 101